Two dimensional localization of electrons and positrons under high counting rate

A. F. Barbosa[(1)] , I. M. Pepe[(2)] , J. C. Anjos[(1)] , A. Sánchez-Hernández[(1)] , N. Barros[(2)]

(1) CBPF, Rua Dr. Xavier Sigaud 150, 22290-180, Rio de Janeiro, Brazil

(2) Instituto de Física, UFBa, Rua Caetano Moura 123, 40210-240, Salvador, Brazil

Abstract

The construction of two wire chambers for the experiment E831 at Fermilab is reported. Each chamber includes three wire planes - one anode and two orthogonal cathodes - in which the wires operate as independent proportional counters. One of the chambers is rotated with respect to the other, so that four position coordinates may be encoded for a charged particle crossing both chambers. Spatial resolution is determined by the wire pitch: 1 mm for cathodes, 2 mm for anodes. 320 electronic channels are involved in the detection system readout. Global counting rates in excess to 10^7 events per second have been measured, while the average electron-positron beam intensity may be as high as 3×10^7 events per second.

Keywords: MWPC, high counting rate, dead-time losses, 2D localization

1. Introduction

FOCUS E831 (“Photoproduction of Charm in an Upgraded Spectrometer”) is an upgrade for the experiment E687 [1,2] at the Fermi National Accelerator Laboratory (Fermilab). In this experiment, the interaction of photons with a Beryllium target at energies around 300 GeV is analyzed in a spectrometer. The aim is to reconstruct a large sample of events containing the charm quark. The upgrade consisted in improving the quantity and quality of analyzed data, specifically by running at higher luminosity and enhancing the efficiency of the detectors and data acquisition system. High energy photons are produced by the Bremsstrahlung method [3]: electrons and positrons are brought to hit a radiator, after which a photon flux is available to interact with an upstream target. The detectors here described are placed right before the radiator, so as to encode the position of electrons and positrons in two dimensions. The contributions of these detectors to the experiment include: help in algorithms for primary vertex reconstruction, beam tagging in events with more than one particle per RF bucket, and improving the resolution in transverse momentum for the inclusive charm production.

2. Detectors description

Each detector is essentially a Multiwire Proportional Counter (MWPC) in which anode wires operate as independent proportional counters. Two orthogonal cathode wire planes are provided at each side of the anode plane, in order to sample avalanche induced signals. A schematic view of the electrodes in the active region of the chambers is shown in Fig. 01. The wire pitch is 2 mm for the anode and 1 mm for the cathodes. The anode-to-

cathode and the cathode-to-window gap is 3.2 mm. The wires diameter is 20 μm, except for guard wires. The active area is 6.4 cm^2, and the windows are made of 300 μm thick carbon fiber. The operating gas is Ar + 25% Ethane, 3 Psi above normal pressure. Since the beam intensity is very high ($\approx 10^7$ particles per second), a drift field has to be established between the cathode plane and the carbon fiber window, in order to avoid charging up of the wires. It has been noted that at least 400 Volts must be applied between cathodes and windows, if long term stability was to be assured at this beam intensity. The anode to cathode voltage for proportional mode operation was around 2100 Volts.

MWPC's designed to cope with counting rates close to 10^7 counts/s per wire have been reported [4], which make use of a special gas filling (CF_4 with hydrocarbons) and a very thin (<1mm) anode-to-cathode gap. However, the average counting rate expected for the application here considered is $\approx 10^6$ counts/s per wire. As it is shown in Section III, this requirement has been met with the construction and operating conditions above described.

A 300 GeV electron or positron loses energy in the gas by two main processes: collisions and radiation. Considering Argon at normal pressure as the operating gas, the Bethe-Bloch corrected formula gives for the energy loss:

$$\left[-\frac{dE}{dx}\right]_{collision} \approx 3 MeV \frac{cm^2}{g}$$

This expression only includes collision losses. Another contribution to the energy loss at this energy range comes from the Brehmsstrahlung process:

$$\left[-\frac{dE}{dx}\right]_{bremms.} \approx 20GeV\frac{cm^2}{g}$$

The effective gas thickness in the detector is about 10^{-3} g/cm^2. This would imply energy loss of 3 KeV by collisions and 20 MeV by Brehmsstrahlung radiation. However, the radiation length (distance over which the particle energy is reduced by a factor 1/*e* due to radiation loss only) is in this case greater than 120 meters, so that the probability for electrons to radiate while crossing the gas thickness is quite low. The probability for radiation in the detector windows is also very low, since their thickness is also much smaller than the radiation length. The effective thickness of both detectors is below 2% of a radiation length. This feature assures that the radiated photons come from the experiment radiator rather than from interactions with the detector parts. In this same thickness, about 60 ion pairs are generated due to collisions. Since the gas pressure is actually slightly above normal pressure, the total number of ion pairs produced by a passing particle is close to 10^2. This is approximately the amount of charge generated by the absorption of a soft x-ray photon in the gas chamber, and such a photon source has been used in characterization tests and measurements.

2.1 Position Measurement

When a particle passes through one of the detectors, the deposited electric charge is driven to an anode wire. The avalanche process occurs, since the anode wires operate as proportional counters. One position coordinate is therefore associated to the position of the wire having registered an avalanche electric pulse. In the orthogonal cathode wire planes,

an avalanche induced charge distribution is spread over several wires. The center-of-gravity of these wires is related to the two-dimensional localization of the particle.

Due to the high beam intensity, it is likely that two or more particles deposit energy on the same wire within a short time interval (<< 1 μs). In this case there would be ambiguity in the position encoding. To deal with this situation, the second detector is rotated with respect to the first one, so that two other coordinate measurements are provided and help lifting out ambiguities. Simulation of random events crossing both detectors indicated that a rotating angle of 30 degrees is adequate for this purpose. Fig. 02 illustrates the connection of individual wires to the operating voltage and the coupling to pre-amplifiers. 64 wires are active for each cathode plane, and 32 for each anode plane. A total number of 320 signal processing channels are therefore involved in the position readout.

2.2 Signal Processing

As shown in Fig. 02, each wire is set to its operating voltage through a biasing resistor. The voltage drop due to the detection of a particle is decoupled by a capacitor that connects it to a voltage pre-amplifier. The shaping time-constant is defined by the pre-amplifier's input impedance paralleled with the biasing resistor, and by the wires capacity. This time-constant is adjusted so that output pulse duration is ≈100 ns, in order to avoid piling up of pulses under high counting rate. Fig. 03 shows the circuit diagram for the pre-amplifiers. Since anode wires get the avalanche charge, while several cathode wires share the charge distribution induced by the avalanches, the amplitude of cathode wire pulses is

lower. The potentiometer at the input stage of the pre-amplifier circuit allows one to gain-tune each channel, so that all channels could have the same output amplitude. Seven pre-amplifiers are implemented in a printed circuit board cards, ten such cards are plugged to a mother board. Five mother boards are therefore enough for both detectors, with extra channels available for replacing eventually dead channels.

Fig. 04 illustrates the remaining signal processing modules. The discriminators are leading edge trigger circuits (16 channel amplifier + discriminator VME cards) which were developed at Fermilab and used in previous experiments. For every detected particle, the wires being hit generate ECL logic pulses at the corresponding discriminators outputs. The state of the wires is then available at the inputs of a latch register. However, the states are latched only when a master gate signal is present. The master gate is the signal that indicates to all other detectors in the experiment that a charm photoproduction event has occurred. It is generated after the photons are produced in the radiator position. To accomplish this operation scheme, fast 16 channel comercial CAMAC time-to-digital converters are used in *common start* or *common stop* mode, with the master gate as the common signal. Besides latching the state of the wires hit by a particle, this scheme allows one to evaluate the time distribution of the signals.

The pre-amplifiers and discriminators are placed close to the detectors. Halfway between the experimental hall and the data acquisition room, ten 32 channel repeater modules are provided to re-shape the discriminator output signals. In the control room the time-to-digital converters are read and data are stored for off-line image reconstruction and analysis.

3 Results

3.1 Thirty wires prototype

In order to evaluate the capability of the proposed detectors for high counting rate applications, a prototype has been built with 30 active anode wires. In this case we were mainly concerned with counting rate measurements, and no cathode planes were used. All other geometrical parameters were the same as described in Section 2.

By illuminating the prototype with x-ray photons from a Cu tube generator, it has been verified that a maximum count rate of 1.2 x 10^6 events per second may be reached at each wire. Fig. 05 shows data corresponding to the measurement of a beam profile for which the global counting rate was close to 2 x 10^7 events per second. By conveniently attenuating the beam intensity and varying the the x-ray tube current, the linearity between true and measured counting rates has been monitored for one of the wires. The corresponding data are plotted in Fig. 06 [5].

Assuming that the true counting rate varies linearly with the x-ray tube current, it has been possible to estimate it by applying a correction to the measured counting rate. A non-paralyzable model has been used for evaluating dead-time losses. The dead-time value was left as a free parameter in the fit of the corrected counting rate to a straight line. This procedure has allowed us to check the *true vs measured* counting rate linearity relation up to 10^6 counts/s per wire. Above this rate the non-paralyzable model was not applicable. Fig. 07 summarizes the obtained results. The dead-time value was found to be 715 ns. This is dominated by the used discriminator output pulse duration: 500 ns.

Under the eletron-positron beam at the experimental hall, the maximum observed counting rate for one wire was ≈ $1.5x10^6$ events per second. This is higher than the observed with the prototype, in particular due to the fact that the energy deposited by the particles (≈ 3 KeV) is lower than in the case of x-ray photons (8 KeV) absorption. In the experimental hall setup, the pre-amplifier and the discriminator output signals were also faster (< 100 ns duration).

3.2 Measurements at the Experimental Hall

The two detectors here described have been acquiring data for the last 1-2 months of beam time available for the experiment run. Updated beam profiles were shown and are accessible in the Internet home page of the experiment (detectors named OGUM1 and OGUM2). 500 million raw events have been recorded and are presently being analyzed. Fig. 08 is a 3D view of the beam profile after image reconstruction, obtained from data corresponding to events triggered by the master gate signal during 2 beam spills (≈ 2 minutes). In the reconstruction algorithm it is required that every recorded event be observed by both detectors. This beam profile reasonably agrees with Monte Carlo simulation of the distribution of electron hits on the radiator.

As expected, for a charm photoproduction event there is a probability that more than one particle have correspondingly passed through the detector. Fig. 09 is a plot of the number of counts - triggered by the master gate - as a function of the number of coincident events observed by the detectors. The plot refers to data collected during 2 beam spills.

Conclusion

Although the detectors have only started to operate during the last two months of the experiment run, a large amount of data has been acquired and is now availble for analysis and image reconstruction. Important experience has been acquired during the detection system setup, especially in the comissioning of signal processing channels, that shall be useful in case of a future experiment run, or in other similar applications. The detectors are relatively simple MWPC's operating in moderate conditions, which have proved to be reliable in supporting very high counting rates, and could certainly be used in other high or low counting rate applications requiring 2D localization of particles. In order to obtain higher counting rates with negligible dead-time losses, an upgraded version of the detectors should be prepared, with smaller anode-to-cathode gap and a faster operating gas. The pre-amplifiers could also be re-engineered to provide faster output pulses.

Acknowledgements

We are grateful to many people who have contributed to the accomplishment of the work here presented: Julio Criginski (Unicamp - University of Campinas), Mônica Gerolimich (CBPF), Cristiana Tribuzy (PUC, Catholic University, Rio de Janeiro), Edilson Tamura (LNLS - National Laboratory for Synchrotron Light), Fernando P. Pinho (CBPF), João P. Pinho (CBPF), Hélio Nigri (CBPF), Germano P. Guedes (CBPF), and the colleagues in the FOCUS Colaboration. Finantial support was due to the CBPF Directory

and to the CNPq (Brazilian National Counsil for Research and Technology Development, PADCT Instrumentation Program).

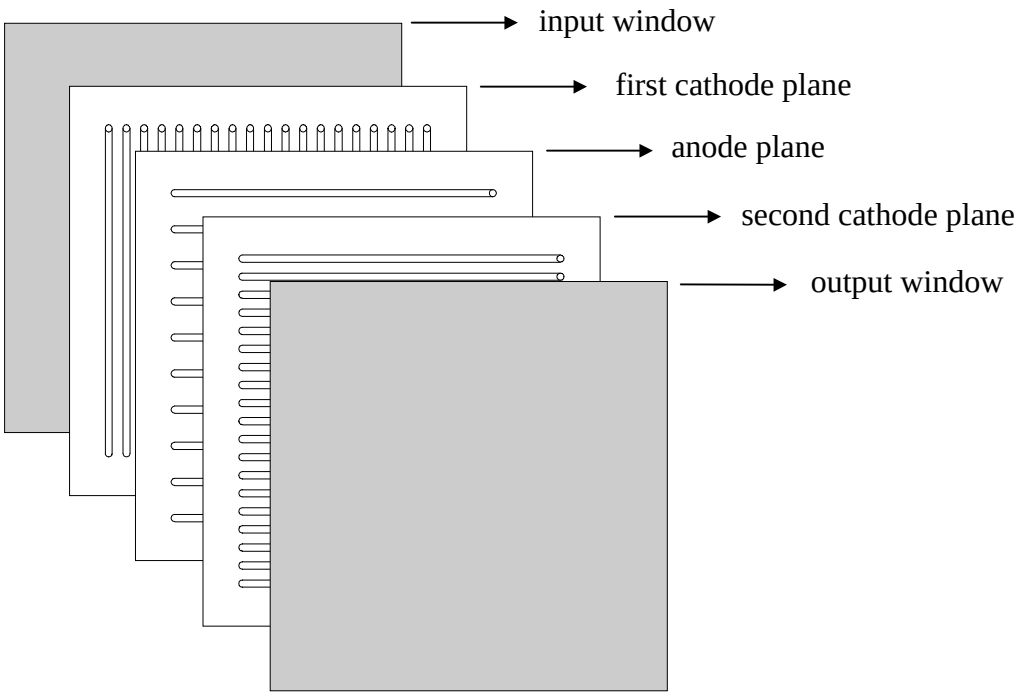

Fig. 01: Schematic view of the electrodes and windows arrangement in the gas chamber.

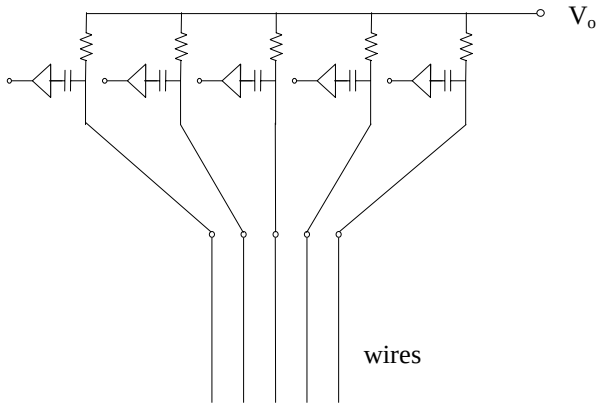

Fig. 02: Illustration of the connection of individual wires to the operating voltage, with coupling to the pre-amplifiers.

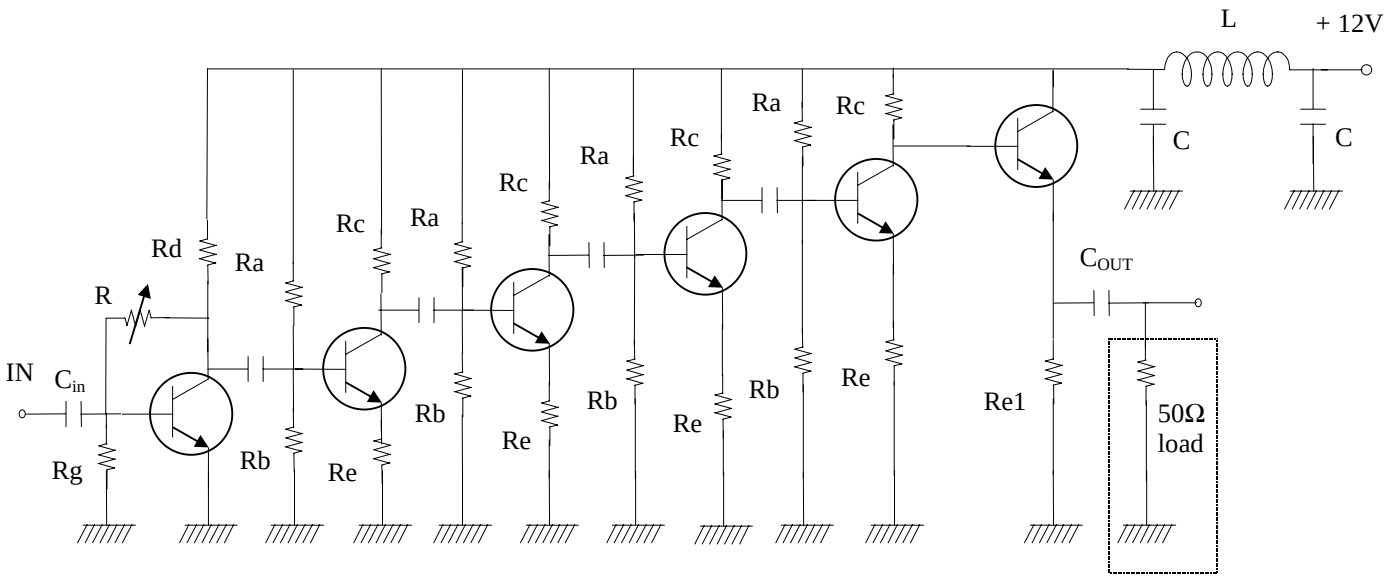

R=50KΩ, Ra=5.6KΩ, Rb=Rc=Rg=1KΩ, Re=220Ω, Re1=120Ω, C_{in}=C_{out}=150pF, Transistors=2N2369A

Fig. 03: Basic circuit diagram for the pre-amplifier circuit.

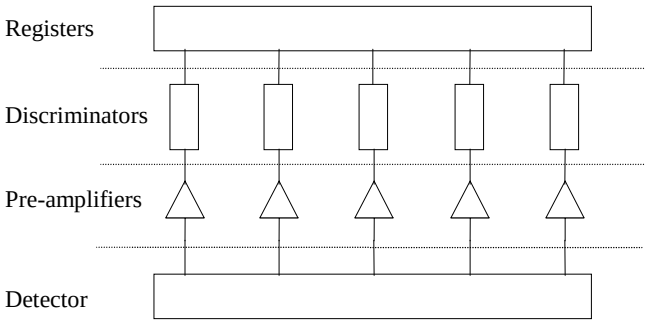

Fig. 04: Partial representation of the signal processing units.

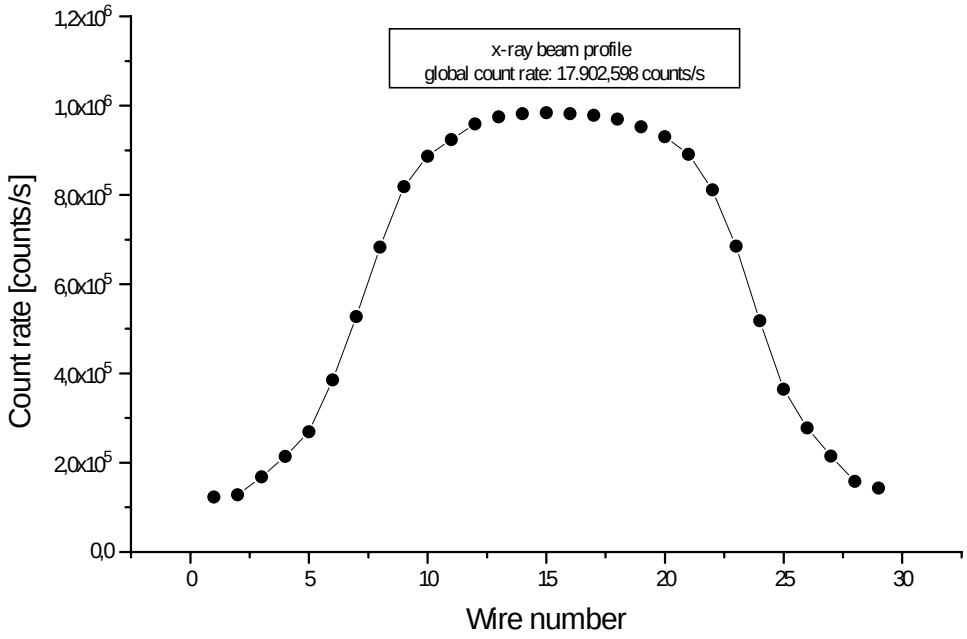

Fig. 05: X-ray beam profile measurement illustrating counting rate capability.

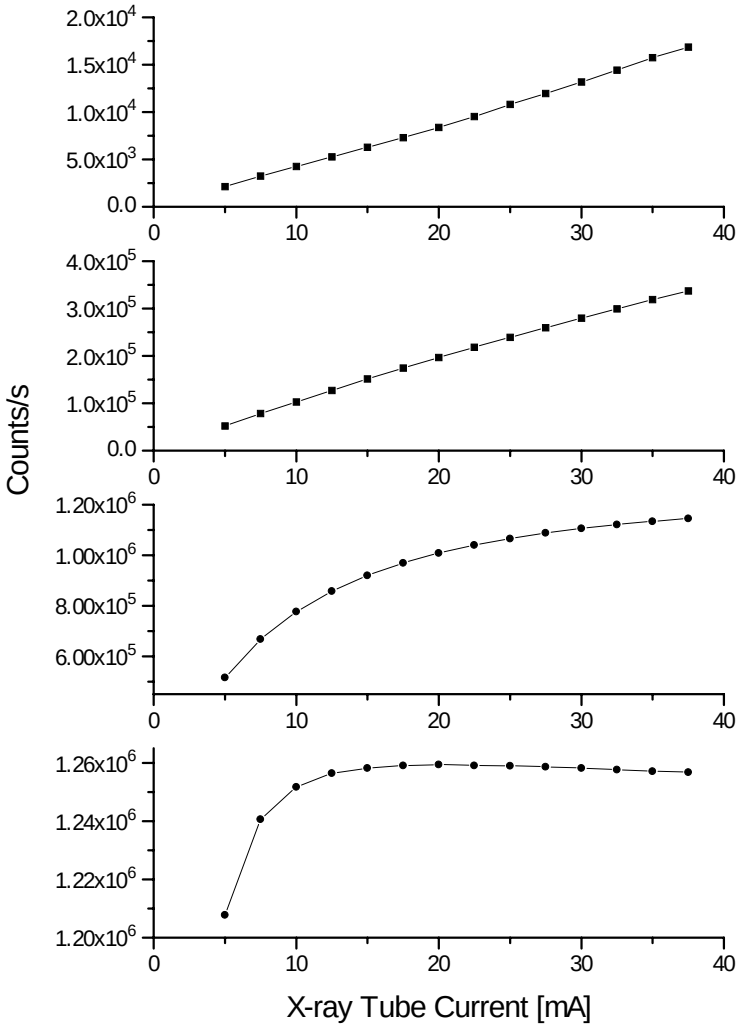

Fig. 06: Plots of linearity measurements for one wire, with counting rates extending from 10^3 to 10^6 counts/s [5].

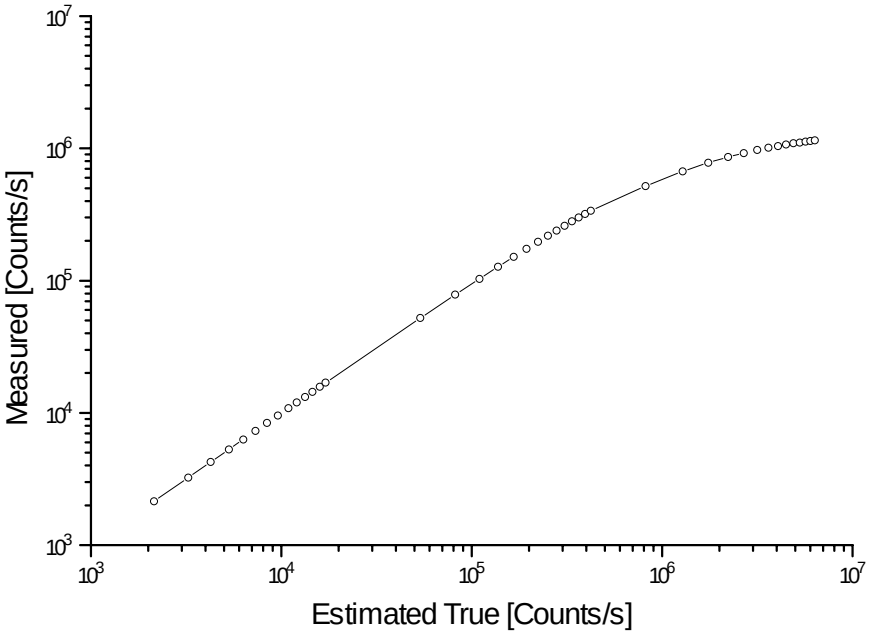

Fig. 7: True *versus* measured counting rate relation for one wire, estimated from the first three sets of data in Fig. 6 by use of a non-paralyzable dead-time model function [5].

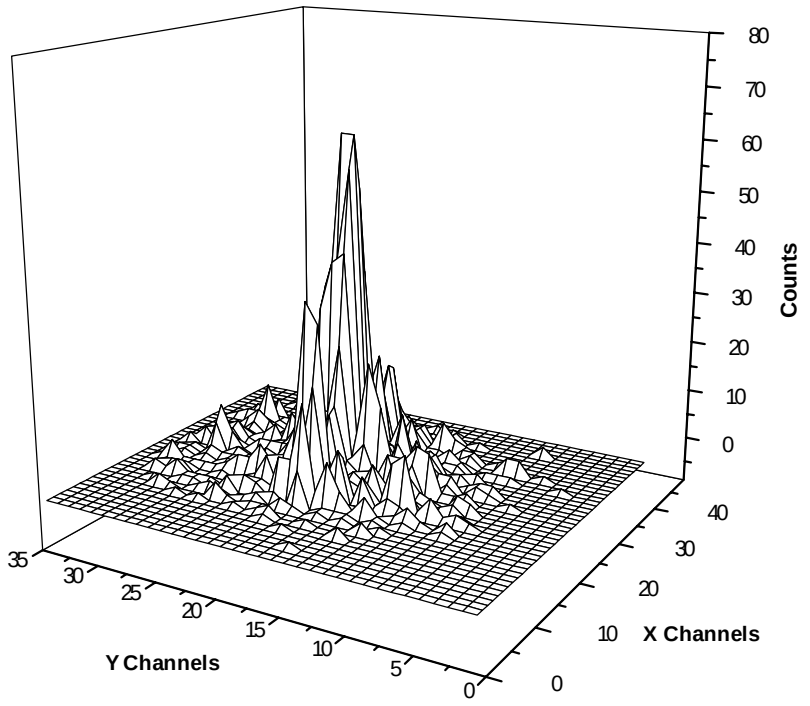

Fig. 08: Beam profile reconstructed from events recorded by both detectors during 2 beam spills.

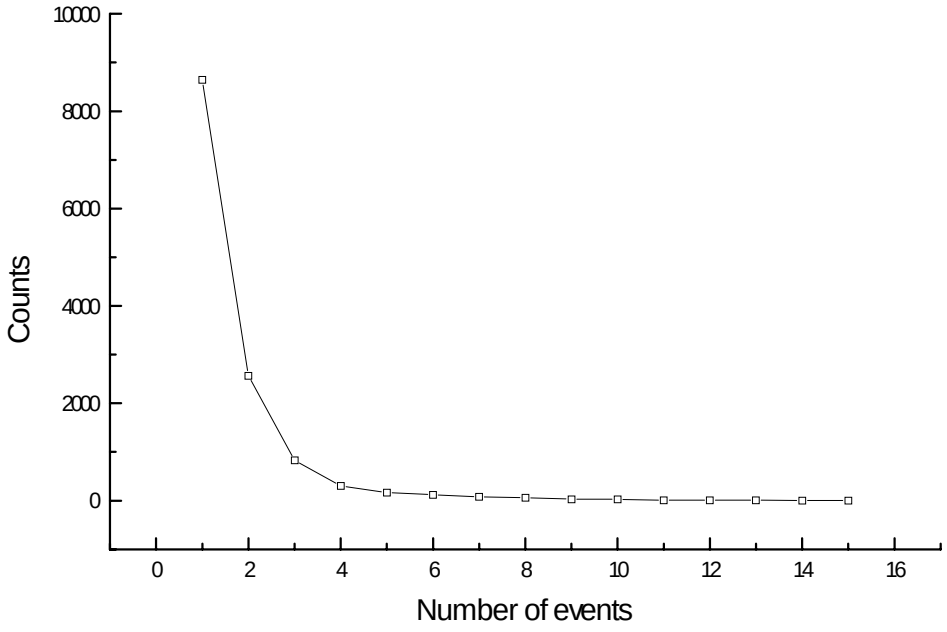

Fig. 09: Distribution of coindident events obtained for data collected in 2 beam spills.

References

[1] P. L. Frabetti et al. *Nucl. Instr. and Meth.* A320 (1992) 519.

[2] P. L. Frabetti et al. *Nucl. Instr. and Meth.* A329 (1993) 62.

[3] J. Buttler et al., Fermilab TM-963 (1980), (updated 1989).

[4] J. Fischer et al., *Nucl. Instrum. and Meth.* A238 (1985) 249.

[5] A. F. Barbosa et al., Proceedings of the *6th International Conference on Synchrotron Radiation Instrumentation*, Himeji-Japan (1997).

Figure Captions

Fig. 01: Schematic view of the electrodes and windows arrangement in the gas chamber.

Fig. 02: Illustration of the connection of individual wires to the operating voltage, with coupling to the pre-amplifiers.

Fig. 03: Basic circuit diagram for the pre-amplifier circuit.

Fig. 04: Partial representation of the signal processing units.

Fig. 05: X-ray beam profile measurement illustrating counting rate capability.

Fig. 06: Plots of linearity measurements for one wire, with counting rates extending from 10^3 to 10^6 counts/s [5].

Fig. 7: True *versus* measured counting rate relation for one wire, estimated from the first three sets of data in Fig. 6 by use of a non-paralyzable dead-time model function [5].

Fig. 08: Beam profile reconstructed from events recorded by both detectors during 2 beam spills.

Fig. 09: Distribution of coindident events obtained for data collected in 2 beam spills.